Electronic Supplementary Material (ESI) for Metallomics.

Supplemental Information

Defining the Mechanism of the Mitochondrial Atm1p [2Fe-2S] Cluster Exporter

Stephen A. Pearson,[1] Christine Wachnowsky,[2] and J. A. Cowan[1,2,3]

Contribution from [1] The Ohio State University Biophysics Program, The Ohio State University, 484 West 12th Avenue, Columbus, Ohio, 43210, [2] The Ohio State University Biochemistry Program, The Ohio State University, 484 West 12th Avenue, Columbus, Ohio, 43210, [3] Department of Chemistry and Biochemistry, The Ohio State University, 100 West 18th Avenue, Columbus, Ohio 43210

Correspondence to: Dr. J. A. Cowan, Evans Laboratory of Chemistry, Ohio State University, 100 West 18th Avenue, Columbus, Ohio 43210. tel: 614-292-2703, e-mail: cowan@chemistry.ohio-state.edu

Experimental Section

Site-Directed Mutagenesis, Protein Growth and Purification

The QuikChange technique (Stratagene) was employed for the following amino acid substitutions: D398A, D398K, D398R, D398E, D398N, and E598A. PCR reactions contained 50 ng of pASK-IBA2 template DNA, 2 units of Phusion DNA polymerase (New England Biolabs), 10x Phusion buffer (New England Biolabs), 125 ng of each primer, 0.2 mM dNTPs, and 3% DMSO. Primers for the mutations were purchased from Integrated DNA Technologies and are shown in Table S1. The thermocycle was identical to that described in the QuikChange manual (Stratagene). The post-thermocycle samples were incubated with 7.5 units of *Dpn*I at 37 °C for 4 h. Subsequently, $CaCl_2$-competent DH5α and BL21 Rosetta cells were transformed via heat shock with the mutant constructs. Mutagenesis results were confirmed by nucleotide sequencing by GENEWIZ.

Protein Growth and Purification

Rosetta(DE3) cells containing the pASK-IBA2 vector with the Atm1p gene were grown in 10 mL LB overnight starter cultures with 100 mg/L ampicillin at 37ºC. This was used to inoculate 1L of LB, which was grown to an OD_{550} of approximately 0.6. Cells were then induced Rosetta(DE3) cells containing the pASK-IBA2 vector with the Atm1p gene were grown in 10 mL LB overnight starter cultures with 100 mg/L ampicillin at 37ºC. This was used to inoculate 1L of LB, which was grown to an OD_{550} of approximately 0.6. Cells were then induced with 20 µg/L anhydrotetracycline. Cells were pelleted after a 24 h induction period at 30^0C. Cell pellets were stored at -80^0C until used.

Approximately 2.5 g of cell pellet was incubated for 30 min in 20 mM Tris, 75 mM NaCl, 10 mM EDTA, pH 8.0 with 1 mg/mL lysozyme. Cell pellet solution was then sonicated and centrifuged at 6,000 rpm (3000 g) for 30 min at 4^0C. The supernatant was removed and centrifuged at 67,000 rpm (150,000 g) for 30 min at 4^0C. The supernatant was removed, and the

pellet resuspended in 10 mL of 20 mM MOPS, 200 mM NaCl, 20% sorbitol, 0.5% *n*-dodecyl β-D-maltoside (ddm), pH 6.5. The solution was homogenized, incubated on ice for 30 min, and centrifuged at 67,000 rpm for 60 min at 4^0C. The supernatant was then removed and diluted 10-fold with 100 mM Tris, 150 mM NaCl, 0.25% ddm, pH 8.0 (buffer W). This was then applied to a StrepTactin superflow column equilibrated with buffer W. The column was then washed with 50 mL buffer W and the protein was eluted with buffer W with 10 mM D-desthiobiotin. Protein samples were concentrated to 2.5 μM, aliquoted, flash frozen, and stored at -20^0C until used.

Primer	Primer Sequence
D398A_FWD	5’-TTTTCTTGGTAGTGTTTACAGAGCTTTAAAGCAGTCTCTGATTGATA-3’
D398A_REV	5’-TATCAATCAGAGACTGCTTTAAAAGCTCTGTAAACACTACCAAGAAAA-3’
D398E_FWD	5’-TTTCTTGGTAGTGTTTACAGAGAATTAAAGCAGTCTCTGATTGATAT-3’
D398E_REV	5’-ATATCAATCAGAGACTGCTTTAATTCTCGTTAAACACTACCAAGAAA-3’
D398R_FWD	5’-TAAATTTTCTTGGTAGTGTTTACAGACGTTTAAAGCAGTCTCTGATTGATATGG-3’
D398R_REV	5’-CCATATCAATCAGAGACTGCTTTAAACGTCTGTAAACACTACCAAGAAAATTTA-3’
D398N_FWD	5’-AAATTTTCTTGGTAGTGTTTACAGACAGTTAAAGCAGTCTCTGATTGATATGG-3’
D398N_REV	5-CCATATCAATCAGAGACTGCTTTAACTGTCTGTAAACACTACCAAGAAAATTT-3’
D398K_FWD	5’-CTAAATTTTCTTGGTAGTGTTTACAGAAAATTAAAGCAGTCTCTGATTGATATGGAA-3’
D398K_REV	5’-TTCCATATCAATCAGAGACTGCTTAATTTTCTGTAAACACTACCAAGAAAATTTAG-3’

Table S1. Primer sequences used in the site directed mutagenesis of the Atm1p gene.

% WT Monomer	% 598A Monomer	WT/WT Dimer	WT/598A Dimer	598A/598A Dimer	One monomer model	Two monomer model
100	0	100	0	0	100	100
75	25	56.25	37.5	6.25	93.75	56.25
50	50	25	50	25	75	25
25	75	6.25	37.5	56.25	43.75	6.25

Table S2. Expected values for cluster transport where either one or two active monomers are required for transport.

The percentage of each dimer in solution was calculated by multiplying the percentages of each monomer together. The amount of WT/WT dimer was calculated by squaring the percentage of WT monomer. The same was done with the 598A/598A dimer. The amount of WT/598A dimer was calculated by multiplying 2 * the percentage of WT monomer * the percentage of 598A monomer. The amount of cluster expected transported in the one active monomer model was determined by adding the percentages of WT/WT dimer plus the WT/598A dimer together. The amount of cluster transported in the two monomer model, where only dimers with two WT monomers, is equal to the amount of WT/WT dimer. The amount of cluster transported in the one monomer model, where only one WT monomer is required for transport, is equal to the WT/WT dimer plus the WT/598A dimer.

	K_D	B
WT	23 ± 3 μM	928 ± 33
D398A	38 ± 10 μM	930 ± 23
D398E	44 ± 7 μM	899 ± 9
D398K	26 ± 7 μM	1023 ± 27
D398N	27 ± 6 μM	919 ± 19
D398R	38 ± 2 μM	1040 ± 25

Table S3: K_D for cluster binding to Atm1p.

Cluster binding affinity (K_D) was also determined through fluorescence quenching experiments by titrating [2Fe-2S](GS)$_4$ cluster into IAEDANS-labeled Atm1p. The weaker affinities relative to Table 1 reflect the absence of MgATP.

ICL Residue	Interacting residue	Interacting residue location	4mrn distance (Å)	4mrv distance (Å)	Difference (Å)
R136A	R136B	ICL1 chain B	2.974	12.375	9.401
R136A	E193A		8.690	2.232	6.972
R136A	E193B		6.487	13.122	4.056
R136A	E493A	Near ABC signature motif Chain A	3.116	10.088	6.458
R136A	E493B	Near ABC signature motif chain B	9.080	5.024	6.635
R130A	E344A		3.288	3.091	0.197
R130A	D371A		3.793	3.851	0.058
R130A	Y411A		5.217	5.066	0.151
H132A	R405A	Same helix as walker A in chain A, near walker B in chain A	4.688	6.049	1.6110
E232B	R405A	Same helix as walker A in chain A, near walker B in chain A	5.634	3.949	1.685
T233B	R510A	Same helix as ABC signature motif in chain A	4.891	4.925	0.034
R136B	R136A	ICL1 chain A	2.974	12.375	9.401
R136B	E193A		6.448	3.556	6.793
R136B	E193B		9.048	13.241	5.492
R136B	E493A	Near ABC signature motif chain A	7.711	5.617	2.094
R136B	E493B	Near ABC signature motif chain B	4.608	14.861	10.253
R130B	E344B		2.543	2.746	0.203
R130B	D371B		4.133	4.183	0.050
R130B	Y411B		5.306	5.289	0.017
H132B	R405B	Same helix as walker A in chain B, near walker B in chain B	7.886	10.052	2.166
E232A	R405B	Same helix as walker A in chain B, near walker B in chain B	5.194	3.581	1.685
T233A	R510B	Same helix as ABC signature motif in chain B	5.518	4.929	0.034

Table S4. Contacts between ICL and NBD residues.

Distances between select resides in the ICL and NBD are shown. Distances are compared in *Na*Atm1p is the absence (PDB ID: 4mrn) and presence (PDB ID: 4mrv) of $Hg(GS)_2$. The letter after the residue number signifies the chain the residue is found in.

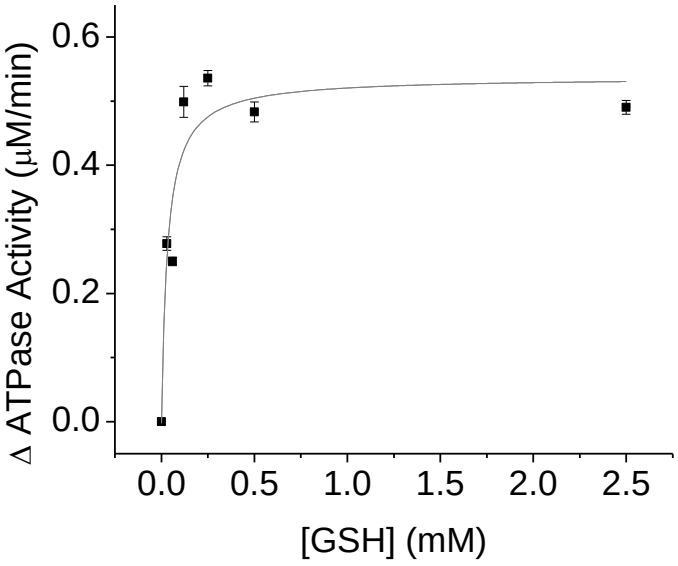

Figure S1: Glutathione dependence of ATPase activity for native Atm1p.

ATPase activity of WT Atm1p at different concentrations of glutathione was measured. K_D for glutathione was calculated to be 32 $\pm$ 9 mM. The increase in ATPase activity was determined to be 0.54 $\pm$ 0.03 μM/min.

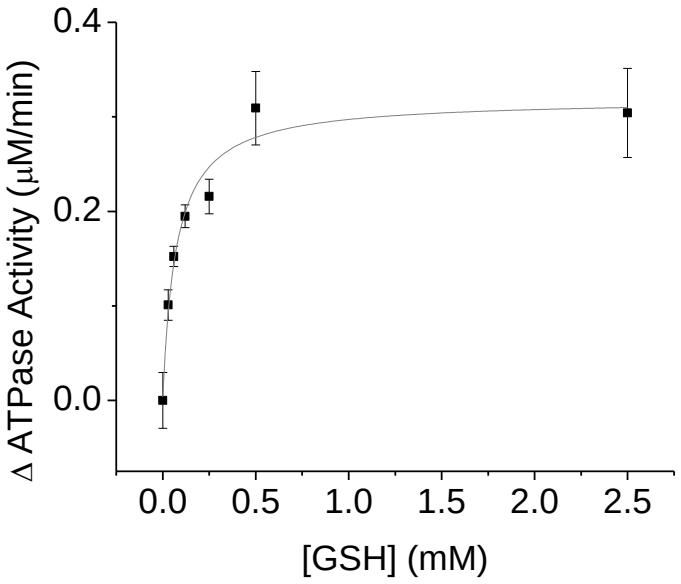

Figure S2: Glutathione dependence of ATPase activity for D398N Atm1p.

ATPase activity of the D398N derivative at different concentrations of glutathione was measured. K_D for glutathione was calculated to be 74 $\pm$ 10 μM. The increase in ATPase activity was determined to be 0.32 $\pm$ 0.01 μM/min.

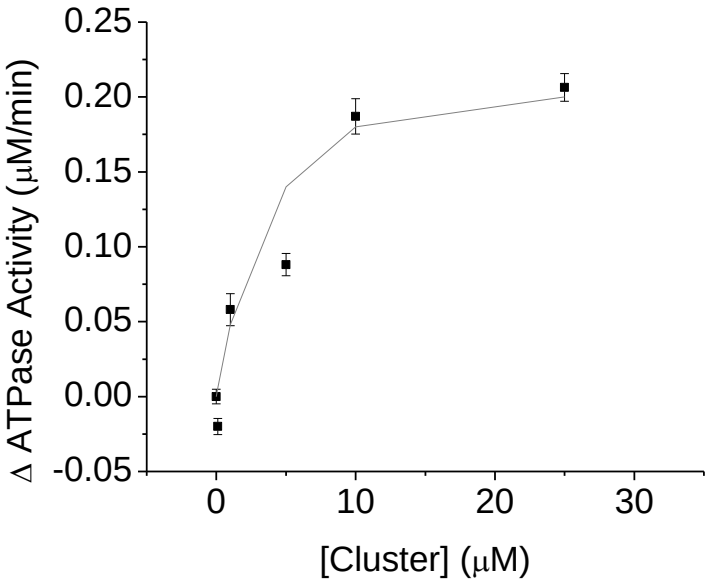

Figure S3: [2Fe-2S](GS)$_4$ dependence of ATPase activity for D398N Atm1p.

ATPase activity of the D398N derivative at different concentrations of cluster was measured. K_D for cluster was calculated to be 5.6 $\pm$ 0.8 μM. The increase in ATPase activity was determined to be 0.36 $\pm$ 0.02 μM/min. Equation 1 was used to fit the data, which accounted for magnesium-induced cluster degradation at high cluster concentrations.

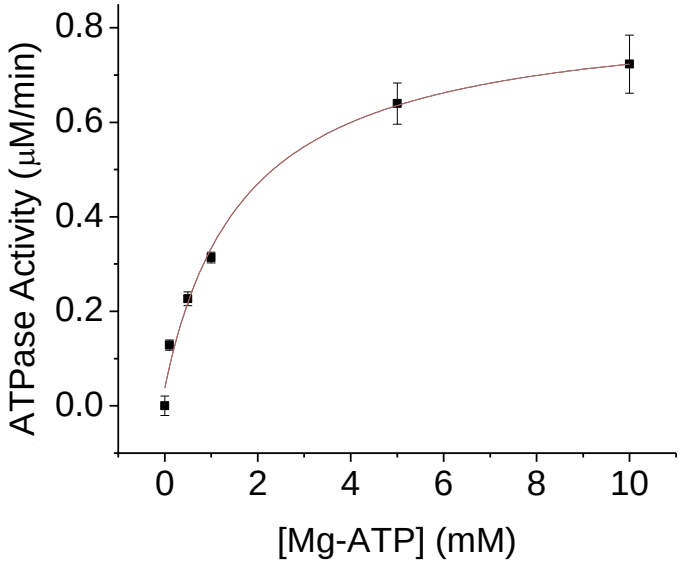

Figure S4: Mg-ATP dependence of Atm1p ATPase activity in the absence of [2Fe-2S](GS)$_4$. ATPase activity of native Atm1p at different concentrations of Mg-ATP was measured in the absence of cluster. The V_{max} was determined to be 0.82 ± 0.04 μM/min, while the K_m for Mg-ATP was determined to be 2.5 ± 0.3 mM.

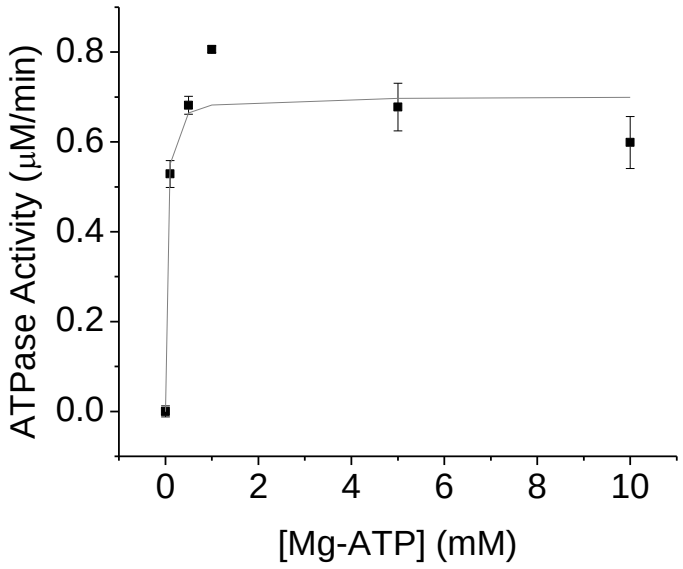

Figure S5: Mg-ATP dependence of Atm1p ATPase activity in the presence of 2.5 μM [2Fe-2S](GS)$_4$.

ATPase activity at different concentrations of Mg-ATP was measured in the presence of 2.5 μM cluster. The V_{max} was determined to be 0.70 ± 0.03 μM/min, while the K_m for Mg-ATP was determined to be 0.027 ± 0.016 mM.

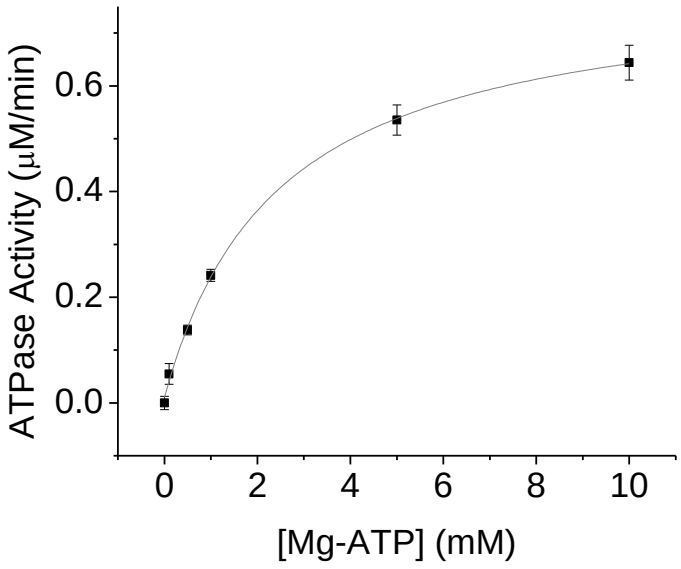

Figure S6: Mg-ATP dependence of Atm1p ATPase activity in the presence of 0.1 μM [2Fe-2S](GS)$_4$.

ATPase activity of native Atm1p at different concentrations of Mg-ATP was measured in the presence of 0.1 μM cluster. The V_{max} was determined to be 0.79 ± 0.01 μM/min, while the K_m for Mg-ATP was determined to be 2.4 ± 0.1 mM.

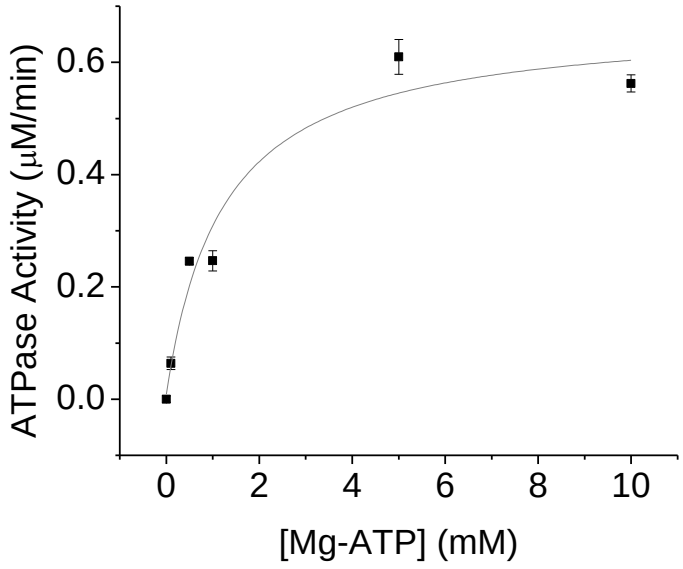

Figure S7: Mg-ATP dependence of Atm1p ATPase activity in the presence of 0.25 μM [2Fe-2S](GS)$_4$.

ATPase activity of native Atm1p at different concentrations of Mg-ATP was measured in the presence of 0.25 μM cluster. The V_{max} was determined to be 0.66 ± 0.04 μM/min, while the K_m for Mg-ATP was determined to be 1.2 ± 0.2 mM.

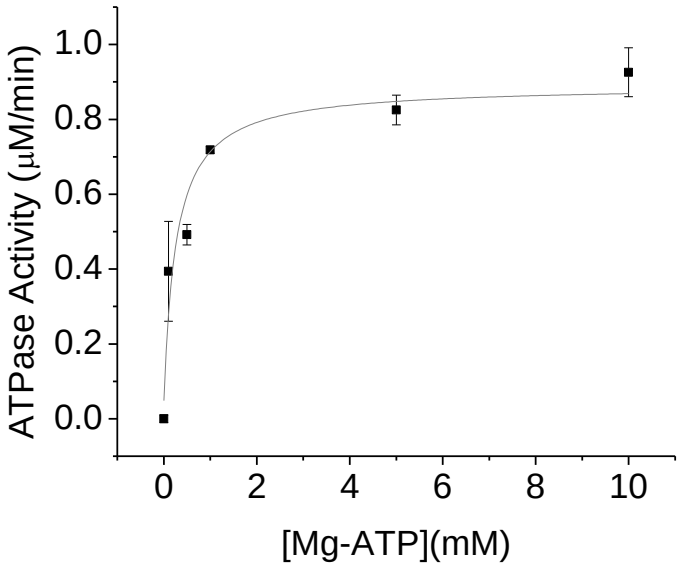

Figure S8: Mg-ATP dependence of Atm1p ATPase activity in the presence of 0.5 μM [2Fe-2S](GS)$_4$.

ATPase activity at different concentrations of Mg-ATP was measured in the presence of 0.5 μM cluster. The V_{max} was determined to be 0.84 ± 0.04 μM/min, while the K_m for Mg-ATP was determined to be 0.27 ± 0.07 mM.

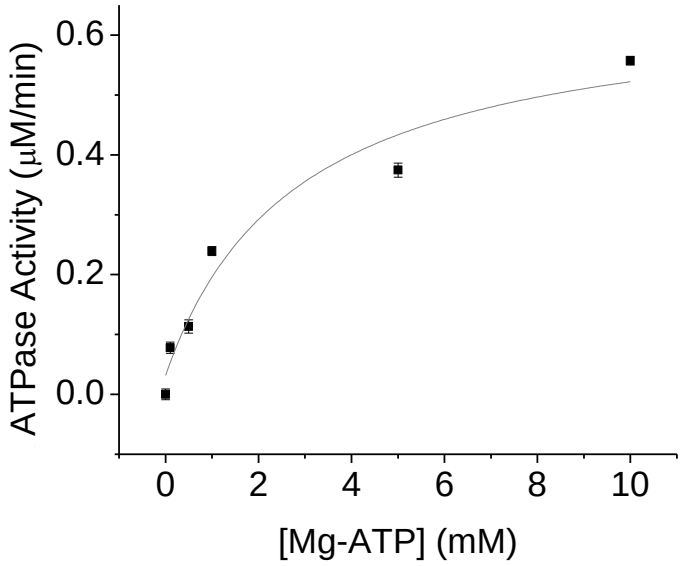

Figure S9: Mg-ATP dependence of D398K Atm1p ATPase activity in the absence of [2Fe-2S](GS)$_4$.

ATPase activity of the D398K derivative at different concentrations of Mg-ATP was measured in the absence of cluster. The V_{max} was determined to be 0.63 ± 0.03 μM/min, while the K_m for Mg-ATP was determined to be 2.8 ± 0.2 mM.

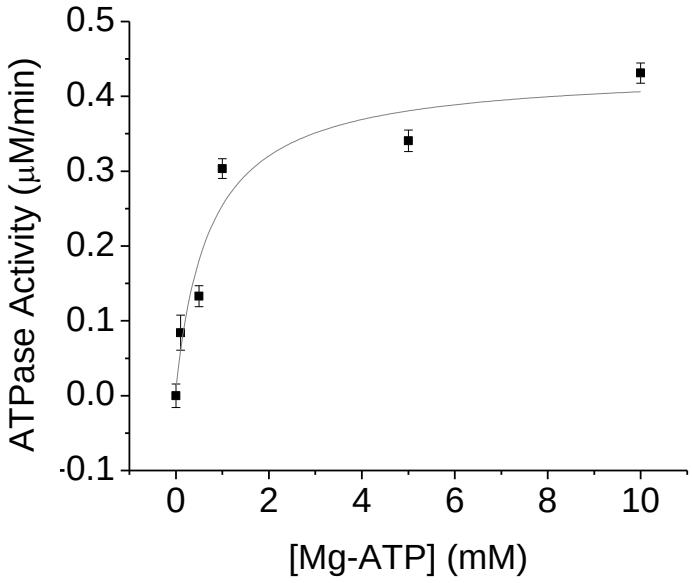

Figure S10: Mg-ATP dependence of D398K Atm1p ATPase activity in the presence of 2.5 μM [2Fe-2S](GS)$_4$.

ATPase activity of the D398K derivative at different concentrations of Mg-ATP was measured in the presence of 2.5 μM cluster. The V_{max} was determined to be 0.42 ± 0.03 μM/min, while the K_m for Mg-ATP was determined to be 0.74 ± 0.18 mM.

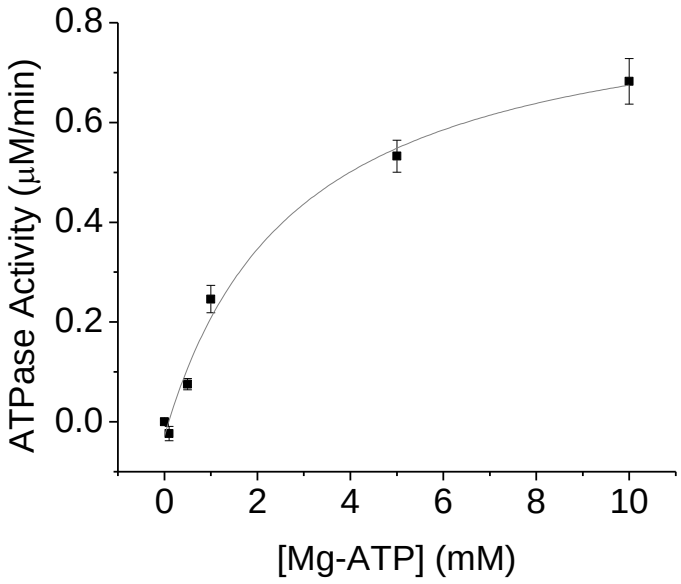

Figure S11: Mg-ATP dependence of D398N Atm1p ATPase activity in the absence of [2Fe-2S](GS)$_4$.

ATPase activity of the D398N derivative at different concentrations of Mg-ATP was measured in the absence of cluster. The V_{max} was determined to be 0.90 ± 0.03 μM/min, while the K_m for Mg-ATP was determined to be 2.8 ± 0.5 mM.

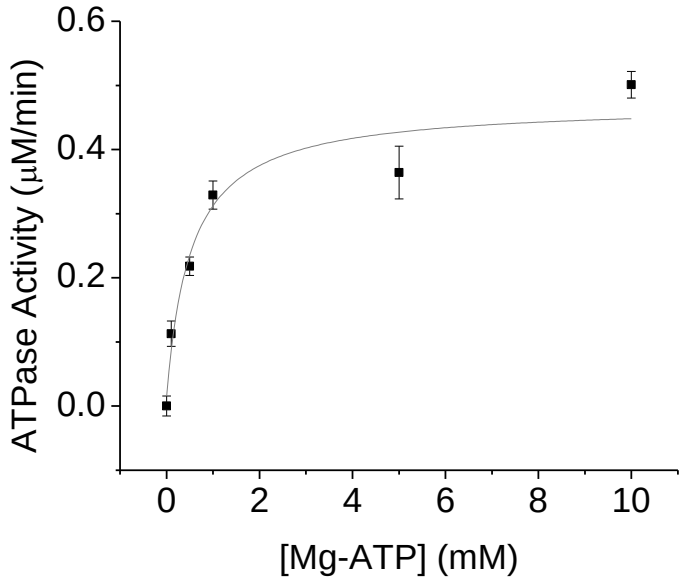

Figure S12: Mg-ATP dependence of D398N Atm1p ATPase activity in the presence of 2.5 μM [2Fe-2S](GS)$_4$.

ATPase activity of the D398N derivative at different concentrations of Mg-ATP was measured in the presence of 2.5 μM cluster. The V_{max} was determined to be 0.46 ± 0.03 μM/min, while the K_m for Mg-ATP was determined to be 0.54 ± 0.12 mM.

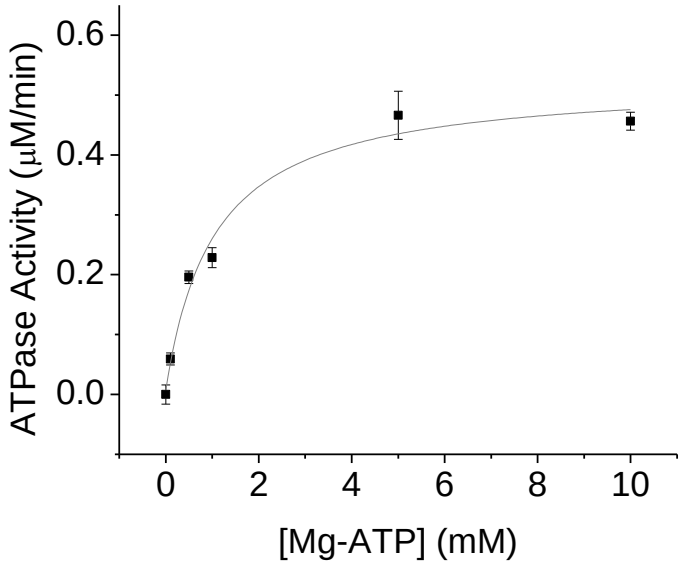

Figure S13: Mg-ATP dependence of D398A Atm1p ATPase activity in the absence of [2Fe-2S](GS)$_4$.

ATPase activity of the D398A derivative at different concentrations of Mg-ATP was measured in the absence of cluster. The V_{max} was determined to be 0.52 ± 0.02 μM/min, while the K_m for Mg-ATP was determined to be 1.0 ± 0.1 mM.

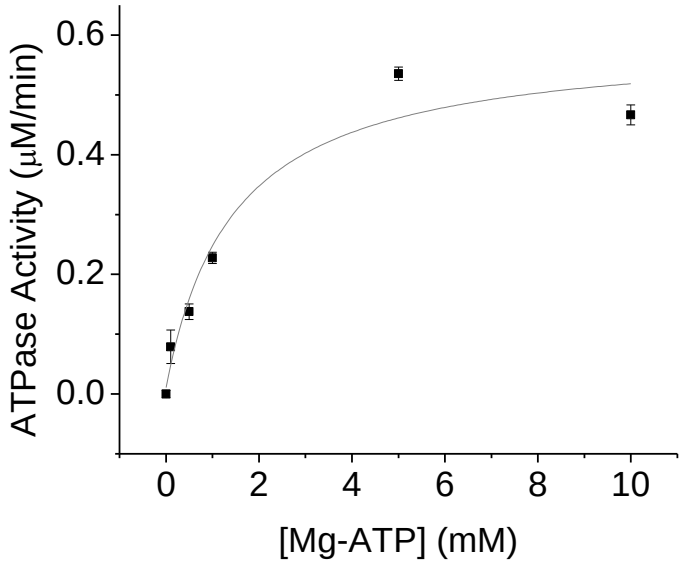

Figure S14: Mg-ATP dependence of D398A Atm1p ATPase activity in the presence of 2.5 μM [2Fe-2S](GS)$_4$.

ATPase activity of the D398A derivative at different concentrations of Mg-ATP was measured in the presence of 2.5 μM cluster. The V_{max} was determined to be 0.58 ± 0.04 μM/min, while the K_m for Mg-ATP was determined to be 1.5 ± 0.3 mM.

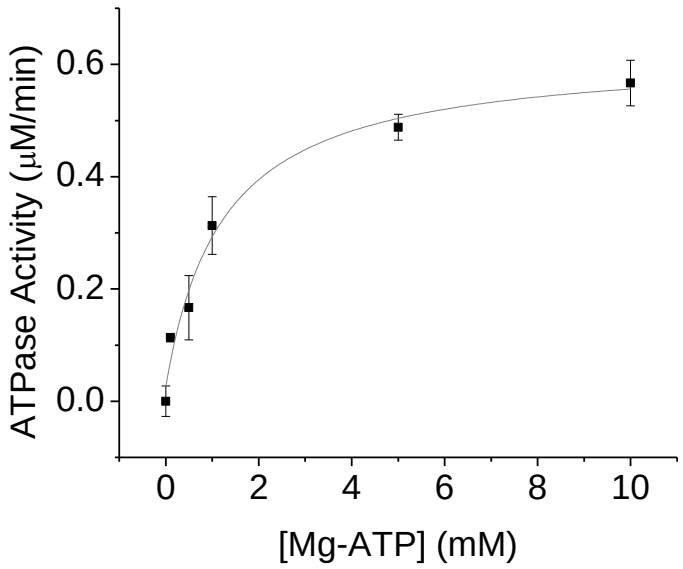

Figure S15: Mg-ATP dependence of D398E Atm1p ATPase activity in the absence of [2Fe-2S](GS)$_4$.

ATPase activity of the D398E derivative at different concentrations of Mg-ATP was measured in the absence of cluster. The V_{max} was determined to be 0.60 ± 0.02 μM/min, while the K_m for Mg-ATP was determined to be 1.2 ± 0.2 mM.

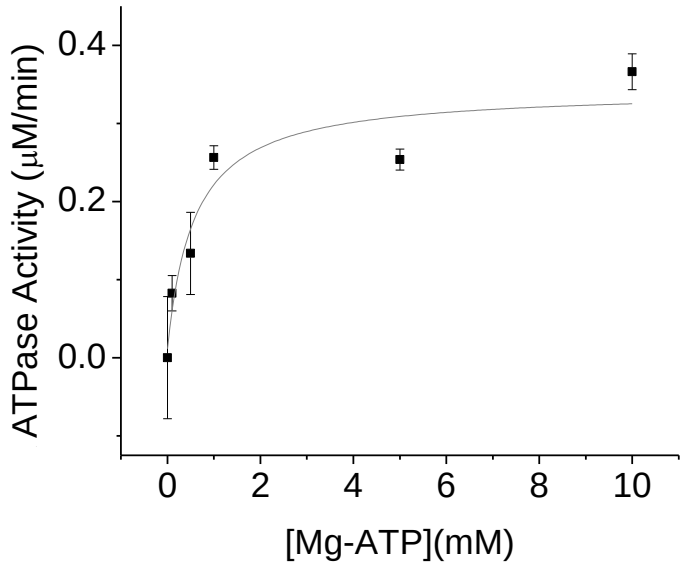

Figure S16: Mg-ATP dependence of D398E Atm1p ATPase activity in the presence of 2.5 μM [2Fe-2S](GS)$_4$.

ATPase activity of the D398E derivative at different concentrations of Mg-ATP was measured in the presence of 2.5 μM cluster. The V_{max} was determined to be 0.33 ± 0.02 μM/min, while the K_m for Mg-ATP was determined to be 0.58 ± 0.18 mM.

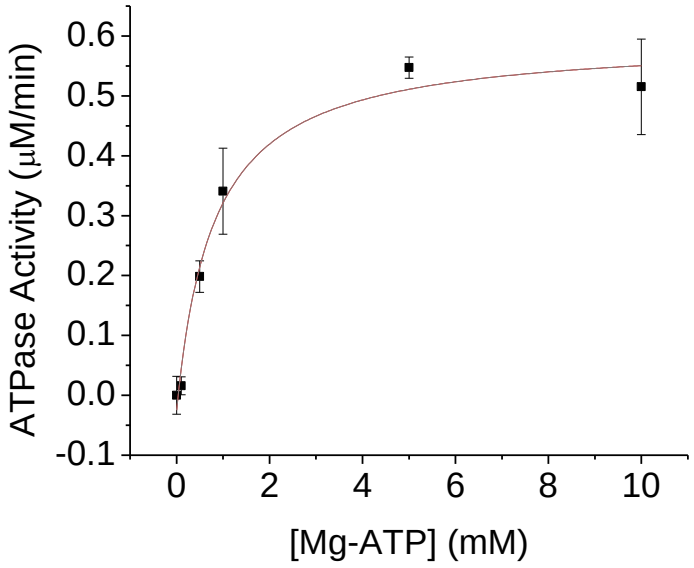

Figure S17: Mg-ATP dependence of D398R Atm1p ATPase activity in the absence of [2Fe-2S](GS)$_4$.

ATPase activity of the D398R derivative at different concentrations of Mg-ATP was measured in the absence of cluster. The V_{max} was determined to be 0.62 ± 0.02 μM/min, while the K_m for Mg-ATP was determined to be 0.80 ± 0.10 mM.

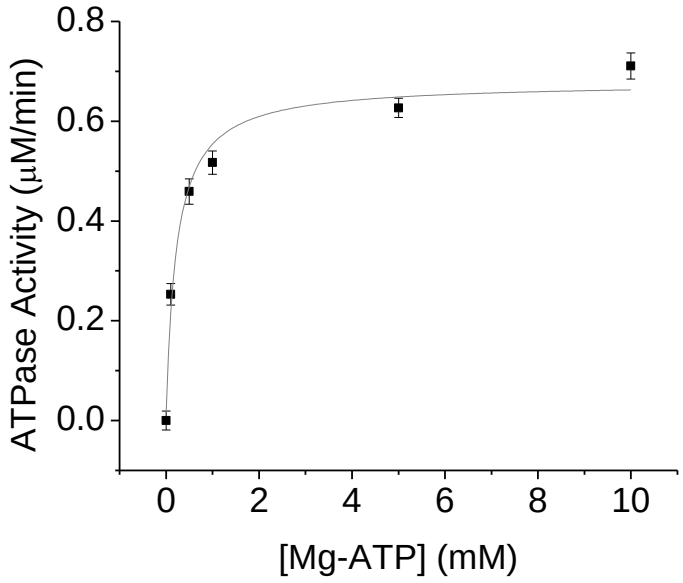

Figure S18: Mg-ATP dependence of D398R Atm1p ATPase activity in the presence of 2.5 μM [2Fe-2S](GS)$_4$.

ATPase activity of the D398R derivative at different concentrations of Mg-ATP was measured in the presence of 2.5 μM cluster. The V_{max} was determined to be 0.66 ± 0.02 μM/min, while the K_m for Mg-ATP was determined to be 0.23 ± 0.03 mM.

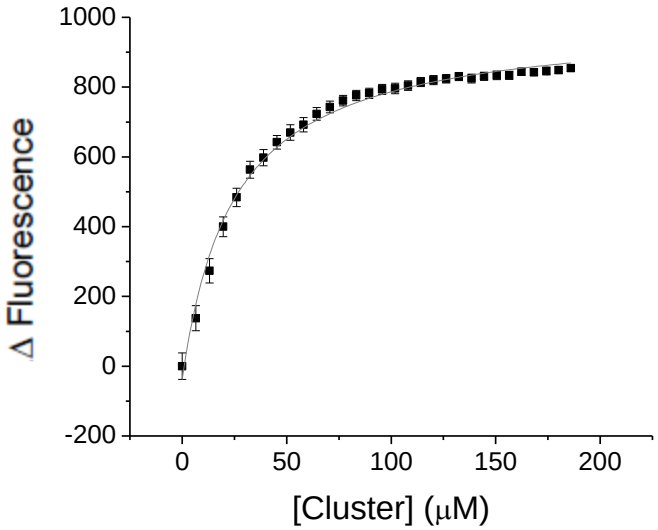

Figure S19: [2Fe-2S](GS)$_4$ binding to native Atm1p.

Cluster binding affinity for WT Atm1p was determined by titrating cluster into labeled Atm1p and was determined to be 23 ± 3 μM.

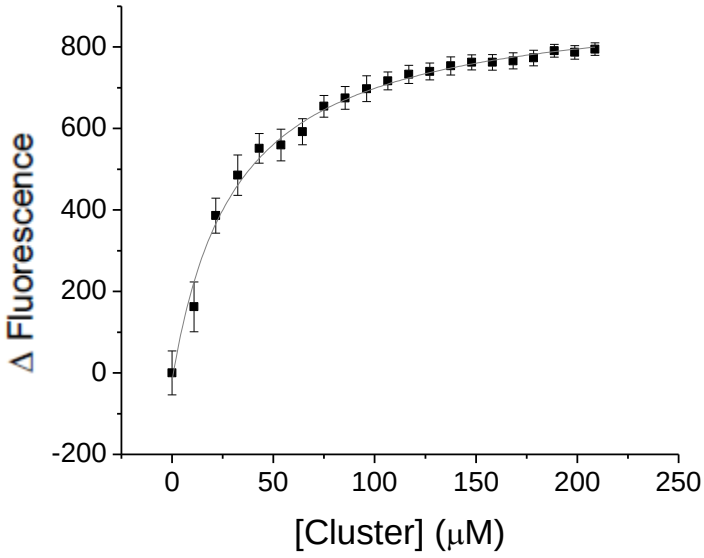

Figure S20: [2Fe-2S](GS)$_4$ binding to D398K Atm1p.

Cluster binding affinity the D398K mutant was determined by titrating cluster into labeled Atm1p and was determined to be 26 ± 7 μM.

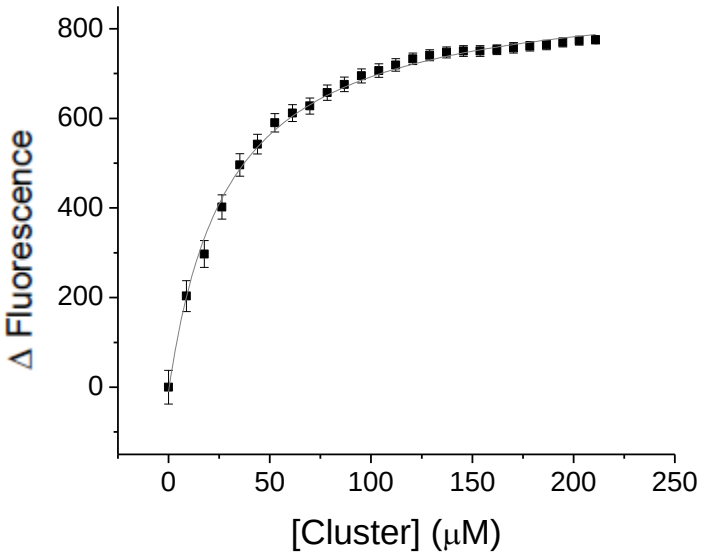

Figure S21: [2Fe-2S](GS)$_4$ binding to D398N Atm1p.

Cluster binding affinity the D398N mutant was determined by titrating cluster into labeled Atm1p and was determined to be 27 ± 6 μM.

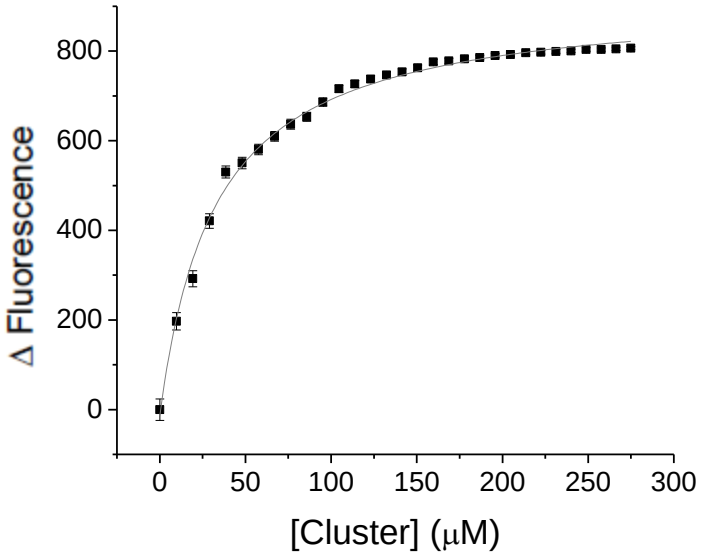

Figure S22: [2Fe-2S](GS)$_4$ binding to D398A Atm1p.

Cluster binding affinity the D398A mutant was determined by titrating cluster into labeled Atm1p and was determined to be 38 ± 10 μM.

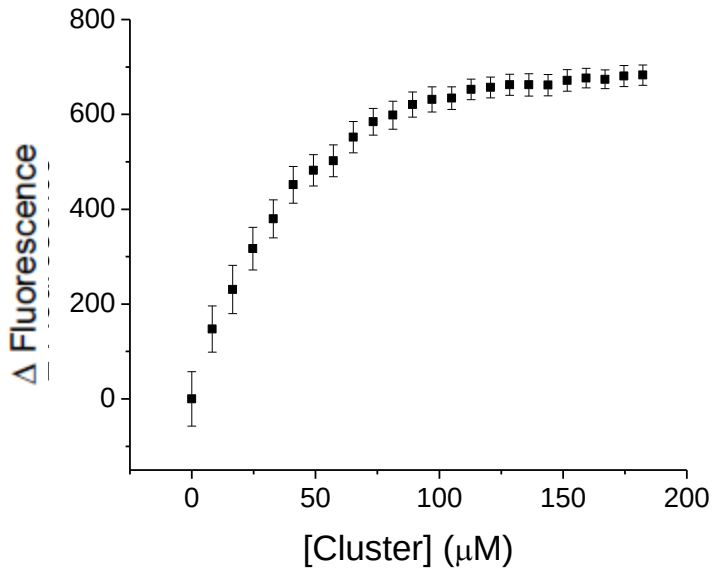

Figure S23: $[2Fe\text{-}2S](GS)_4$ binding to D398E Atm1p.

Cluster binding affinity the D398E mutant was determined by titrating cluster into labeled Atm1p and was determined to be 44 ± 7 μM.

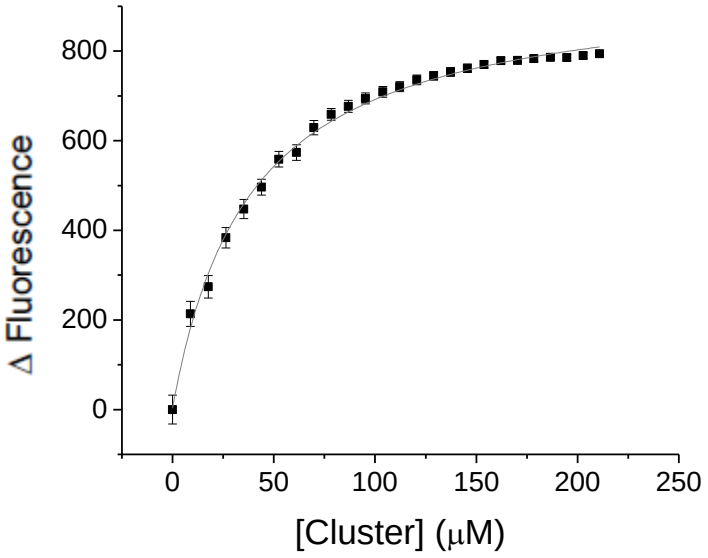

Figure S24: [2Fe-2S](GS)$_4$ binding to D398R Atm1p.

Cluster binding affinity the D398R mutant was determined by titrating cluster into labeled Atm1p and was determined to be 38 ± 1 μM.

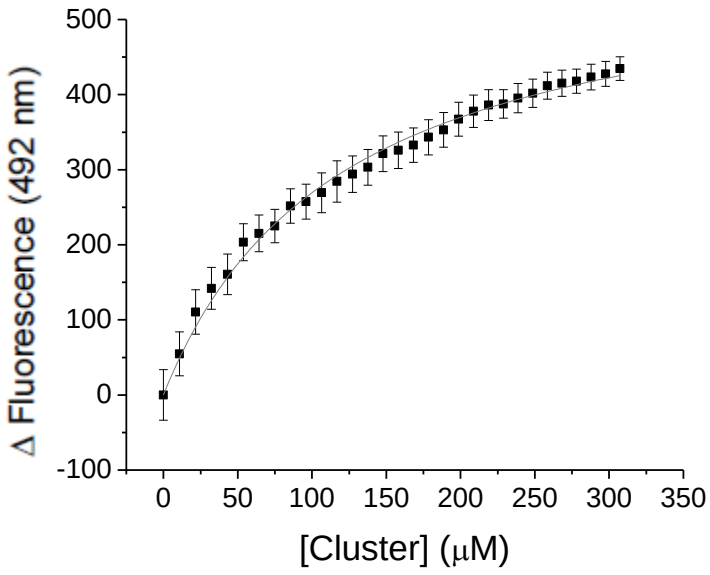

Figure S25: [2Fe-2S](GS)$_4$ binding in the absence of nucleotide.

Cluster binding affinity was determined by titrating cluster into labeled Atm1p in liposomes and was determined to be 119 ± 2 μM.

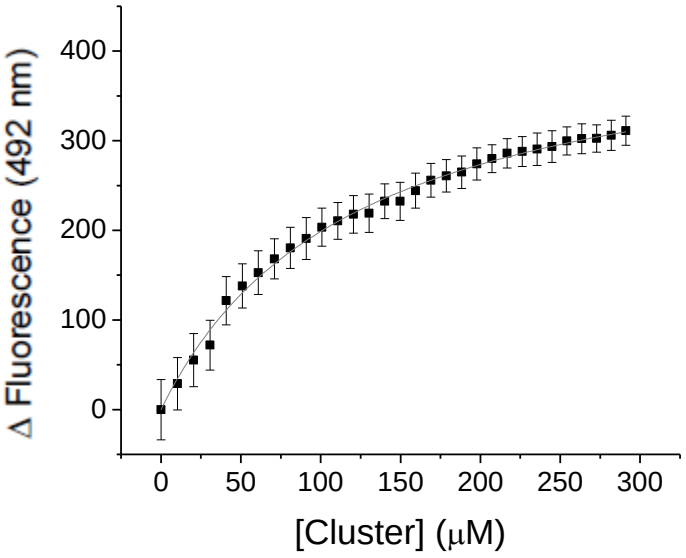

Figure S26: [2Fe-2S](GS)$_4$ binding in the presence of Mg-ADP.

Cluster binding affinity in the presence of Mg-ADP was determined by titrating cluster into labeled Atm1p in liposomes and was determined to be 120 ± 1 μM.

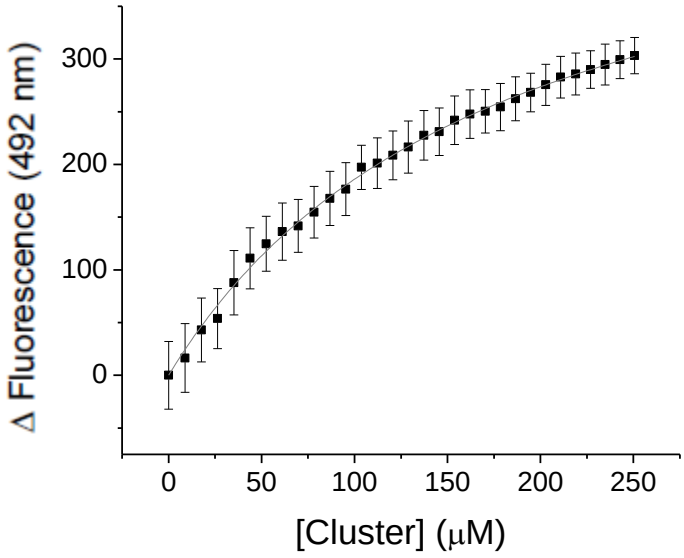

Figure S27: [2Fe-2S](GS)$_4$ binding in the presence of Mg-ATPγS.

Cluster binding affinity in the presence of non-hydrolyzable ATP (ATPγS) was determined by titrating cluster into labeled Atm1p in liposomes and was determined to be 179 ± 7 μM.

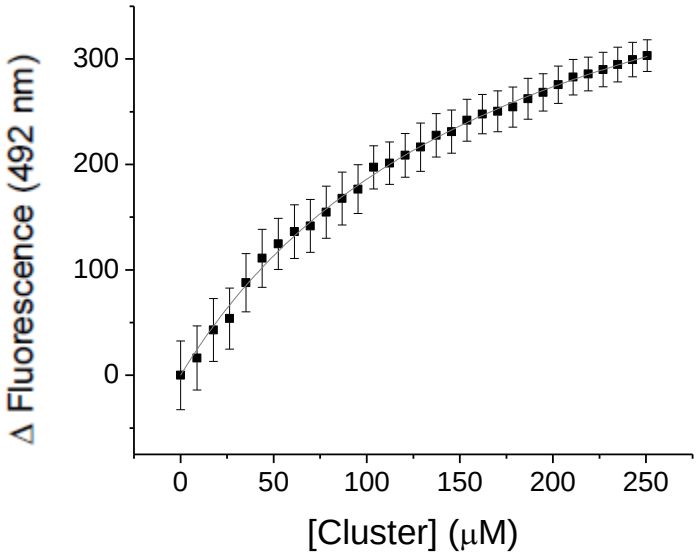

Figure S28: [2Fe-2S](GS)$_4$ binding in the presence of Mg-ATP plus vanadate.

Cluster binding affinity in the presence of Mg-ATP and vanadate was determined by titrating cluster into labeled Atm1p in liposomes and was determined to be 179 ± 1 μM.

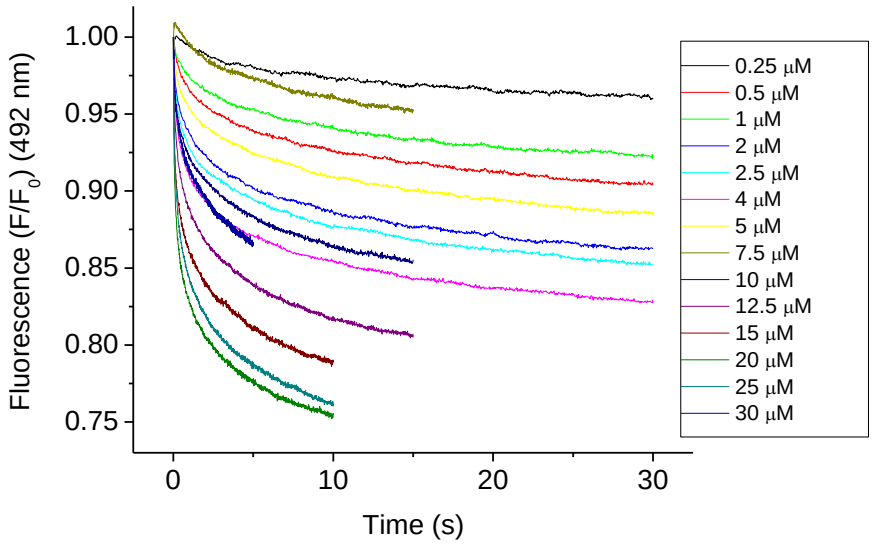

Figure S29: [2Fe-2S](GS)$_4$ cluster binding kinetics

Stopped flow experiments were conducted with IAEDANS labeled Atm1p to investigate the rate of cluster binding at different concentrations of cluster. Data was analyzed with DyanFit4 software to determine the reaction order with respect to cluster (Figure 7, main text).

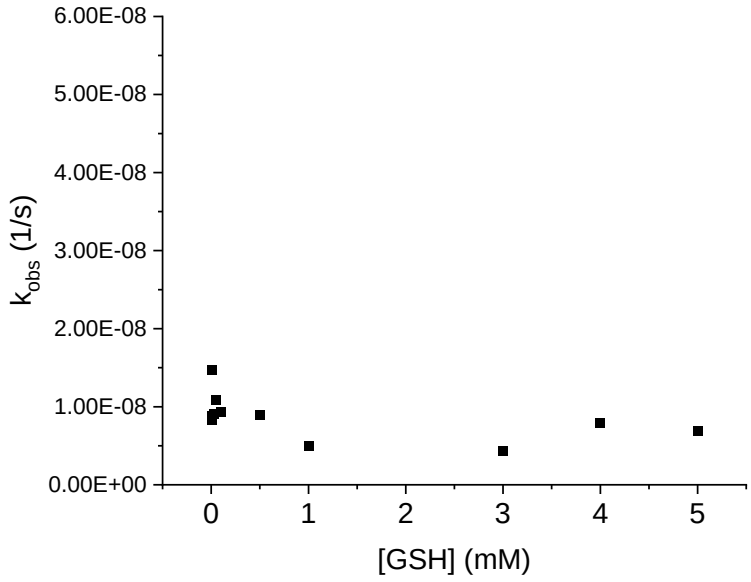

Figure S30: GSH binding kinetics

GSH binding kinetics from stopped flow experiments were analyzed using DynaFit4 software to determine the observed first-order rate constants of binding at different concentrations of GSH (equations 5 and 6, Fig. S31). In contrast to cluster binding ((Figure 7, main text) no second-order term (k_s) was observed when fitting the GSH dependence data because GSH binding did not quench the fluorescence. Only the first-order intramolecular transition (k_i) was detected as the observed rate constant remained relatively unchanged (note the y-axis scale) as cluster concentration increased.

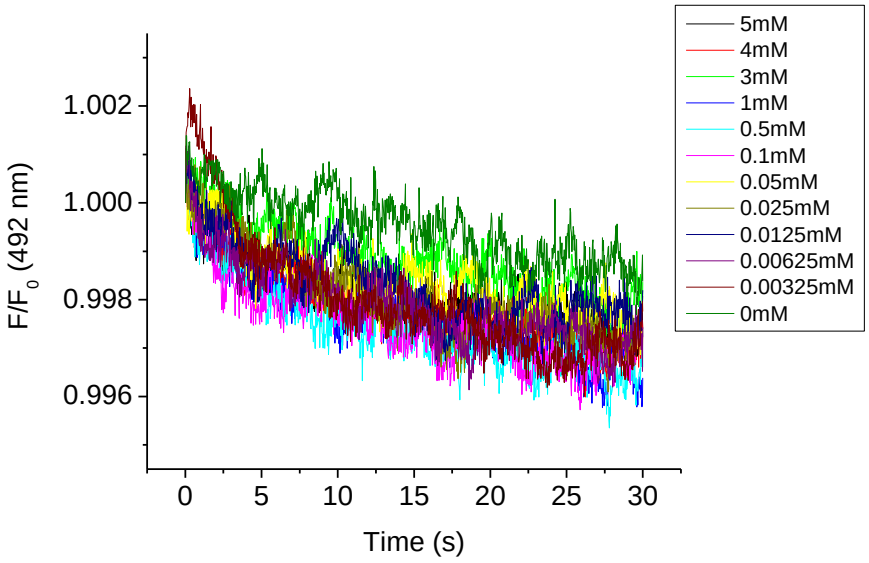

Figure S31: GSH binding kinetics

Stopped flow experiments were conducted with IAEDANS labeled Atm1p to investigate the rate of GSH binding at different concentrations of cluster. Data was analyzed with DyanFit4 software to determine the reaction order with respect to GSH (Figure S30).